ChemElectroChem

Research Article
doi.org/10.1002/celc.202300271

Chemistry Europe
European Chemical Societies Publishing

www.chemelectrochem.org

Laser-Induced Carbon Nanofiber-Based Redox Cycling System

Antonia Perju[a] and Nongnoot Wongkaew*[a]

Redox cycling is a powerful amplification strategy for reversible redox species within miniaturized electrochemical sensors. Herein, we generate three-dimensional (3D) porous carbon nanofiber electrodes by CO_2 laser-writing on electrospun polyimide (PI) nanofiber mats, referred to as laser-induced carbon nanofibers (LCNFs). The technique allowed the fabrication of interdigitated electrode (IDE) arrays with finger width and gap distance of ~400 μm and ~40 μm, respectively, offering approximately 3.5 times amplification efficiency (AF) and 95% collection efficiency (CE). Such dimensions could not be achieved with IDEs fabricated on conventional PI film because the devices were short-circuited. Stacked electrodes were also constructed as an alternative to the IDE design. Here, nanofiber mats as thin as ~20 μm were fabricated and used as vertical insulation between two LCNF band electrodes. While redox cycling efficiency was similar, the IDE design is more favorable considering the lower complexity and better signal reproducibility. Our strategy thus paves the way for creating flexible 3D porous electrodes with redox cycling ability that can be integrated into microfluidics and lab-on-a-chip systems. In particular, the devices offer inherent flow-through features in miniaturized analytical devices where separation and sensitive detection could be further realized.

Introduction

In recent decades electrochemical sensors have gained considerable attention as they generate minimal waste, are fast, inexpensive, easy to operate, and portable. The well-established miniaturization technology has enabled electrochemical sensors to be even more precise, sensitive, and selective to achieve successful integration within micro total analysis (μ-TAS) or lab-on-a-chip systems. Therefore, the detection of a minute sample volume is feasible, facilitating the development of analytical devices for point-of-care (POC) testing. In general, the electroactive surface area (ESA) plays a crucial role in detection sensitivity. Unlike traditional film-like electrodes, three-dimensional (3D) electrodes are highly beneficial in elevating available ESA within a limited space of miniaturized electroanalytical systems.[1–3] Furthermore, with special electrode geometries and designs ones can potentially enable efficient mass transport of the redox species to and from the electrode surface, which results in greater electrochemical signals.[4]

Redox cycling between two adjacent electrodes is one of the most popular amplification strategies for reversible redox species that is widely utilized within miniaturized devices.[5–7] In principle, the strategy enables multiple rounds of the reversible redox reaction by just manipulating electrode designs without the need for additional reagents. Typically, one electrode, called a generator, serves as an initial oxidation or reduction site of an analyte. Subsequently, the as-generated product species diffuses towards the second electrode, called a collector, where a potential is applied to drive the reverse reaction. To successfully accomplish the redox cycling event, the space between the two electrodes is critical. It should be as narrow as possible to promote the overlapping of the diffusion layers, hence facilitating the resulting amplified current.[8] The redox cycling system is also a powerful strategy to enable discrimination of redox species with different reaction characteristics since currents from chemically irreversible redox reactions are not being amplified.[9,10]

Various electrode configurations and designs, both lateral and vertical approaches, have been reported and achieved very good signal amplification efficiencies.[11] Interdigitated electrodes (IDEs) in an array format are one of the most popular configurations due to their simplicity in terms of design and manufacturing. Most research attempts on IDE fabrication have focused on the development of fabrication methods that allow close proximity between electrodes. With traditional photolithography, a few micrometers of gap can be typically obtained,[12,13] whereas with advanced nanolithography, the distance between electrodes at a few hundreds of nanometers was feasible.[14,15] The construction of 3D-IDEs has proven that increasing the electrode height allows one to substantially increase the amplification efficiency as redox species can be trapped in between the two electrodes and thus confine the diffusion within the vertical surface.[16–18] In addition to IDE design, the vertical configuration has also received attention. In particular, a facile construction uses insulating materials sandwiched between two planar macro-band electrodes. The key challenge is, thus, how to make the insulating layer as thin

[a] Dr. A. Perju, Dr. N. Wongkaew
Institute of Analytical Chemistry, Chemo- and Biosensors
University of Regensburg
93053 Regensburg, Germany
E-mail: nongnoot.wongkaew@ur.de

Supporting information for this article is available on the WWW under https://doi.org/10.1002/celc.202300271

as possible. Non-conductive porous layers such as spherical beads[19,20] and paper[10] have been demonstrated as great candidates for generating POC devices owing to their simplicity. However, the previous fabrication techniques inevitably require sophisticated steps and costly facilities and materials, which make them unsuitable for resource-limited areas. Furthermore, their applicability and integration in flow-through analytical devices may be limited.

Laser-induced carbonization by CO_2 laser has recently caught a lot of attention as an efficient and simple strategy to generate graphene electrodes on carbonizable and flexible substrates in a massive and inexpensive manner, which is highly promising for the fabrication of POC devices.[21] Recent works have successfully fabricated IDEs on polyimide (PI) sheet (or Kapton foil) via laser-induced carbonization and demonstrated their capability as an electrochemical transducer in energy storage and sensors.[22–26] Nevertheless, to the best of our knowledge, no investigations on the redox cycling ability of the laser-generated IDEs have been reported so far. In addition, the inter-electrode distances reported were mostly in the range of a few hundred of micrometers, which may be insufficient to promote redox cycling. Therefore, we conducted an investigation towards the possibility of redox cycling on such devices, aiming to strengthen and advance the utilization of the laser-carbonization strategy to ultimately fulfill the demands of POC testing in terms of cost and detection sensitivity.

Carbon nanofibers (CNFs) possess a large surface-to-volume ratio and porosity, assuring an efficient internal mass transfer. They also possess good electrical conductivity, low material cost, and chemical inertness, making them a great candidate as a transducer material in miniaturized electrochemical sensors. Recently, our research group has proposed an efficient method for the fabrication of 3D-CNFs and shown their excellent electroanalytical performance when integrated into miniaturized devices.[1] In our method, electrospun PI nanofibers are exposed to a CO_2 laser under ambient conditions to generate CNF electrodes of arbitrary designs. The available 3D-porous structures and breathability within the laser-induced CNF (LCNF) electrodes not only facilitate efficient analyte-interface interactions but also allow flow-through analytical measurement setup possible either laterally or vertically, which cannot be realized when using a flat PI sheet as substrate. The mechanical and electrochemical stability of the LCNF electrodes have been tested and were found to be sufficient even under strong agitation conditions.[1,27]

In the present work, we therefore propose simple electrode constructions made from LCNFs using both laterally and vertically separated electrodes in which great signal amplification efficiency could be achieved without the need of clean-room facilities or sophisticated fabrication steps. With IDE configuration, the studies were dedicated to the optimization of electrode designs, i.e., width of finger, gaps between fingers, and thickness, to maximize redox cycling efficiency. Furthermore, we found that the use of PI nanofiber mats instead of PI sheets resulted in the smallest obtainable inter-electrode distances and, therefore, superior sensing conditions. With vertically stacked electrodes, a thin layer of PI nanofiber mat was sandwiched in between the two band LCNF electrodes. The influence of fiber mat thickness on redox cycling efficiency was investigated. The two approaches were compared and discussed in terms of the influence of design on redox cycling efficiency and constraints.

Results and Discussion

Electrode designs and electrochemical characterization of LCNF electrodes for redox cycling

In order to characterize the amplification efficiency of the as-fabricated devices, cyclic voltammograms (CVs) of ferrocyanide in single- and dual mode were compared. The single mode utilizes a single array or a band of LCNFs as a working electrode, also called the generator (Figure 1a–i). Here, the diffusion layer expands, and diffusion controlled current in CV is thus obtained (see also Figure 1d–i *violet curve*). On the contrary, the dual mode possesses two working electrodes in which one electrode serves as a generator and another as a collector (Figure 1a–ii). The collector allows the reversible redox reaction to take place. Therefore, when the two working electrodes are close enough, i.e., diffusion layers are overlapping, multiple redox cycling events can occur at the generator, which ultimately facilitates signal amplification. Therefore, the current at the generator becomes steady in this case (Figure 1d-i, *pink curve*). The ratio of currents at the generator in dual mode to single mode indicates the amplification factor (AF). Additionally, as we monitor the current generated at the collector in dual mode, the ratio of currents at the collector to the generator principally implies a collection efficiency (CE) of the redox cycling system. Herein, we evaluated the AF and CE at 0.6 V. Figure 1d–ii shows a representative CV from electrode construction and design, which is unable to facilitate redox cycling even the dual mode is applied. This is mostly resulted from the two working electrodes being too far apart and/or scan rates being too fast in which the as-generated oxidized species do not have sufficient time to reach the collector.

To enable redox cycling on LCNF electrodes, we investigated two distinct construction strategies, namely interdigitated electrode (IDE) array (Figure 1b), and stacked electrodes (Figure 1c). The IDE configuration is proposed as it is simple and requires only a single step in electrode generation. It is also highly practical to implement with lateral-flow assay-based devices. With our electrode fabrication strategy and device assembling approach, the heights of electrodes can be simply tuned by varying the thickness of the nanofiber mat, i.e., through the control of fiber collection time. The challenges associated with such design involve the constraints of commercially available CO_2 laser, which include focal beam size and deviations of electrode sizes from the original assigned dimensions. Therefore, studies were carried out on how electrode designs affected final electrode dimensions, which subsequently influenced redox cycling. Although the stacked electrodes require a few more steps in fabrication, their construction is highly suitable for vertical-flow through assays,

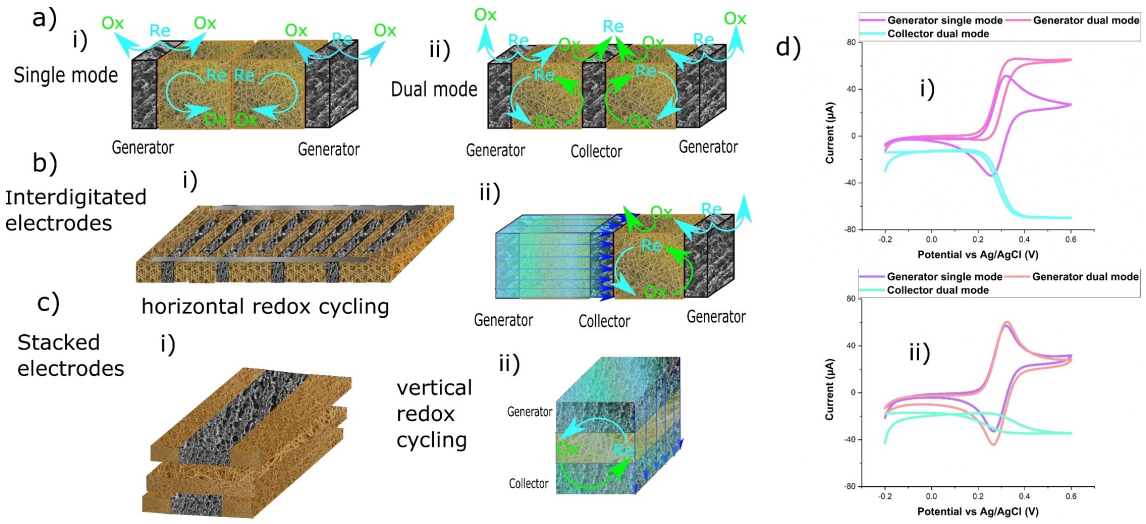

Figure 1. Principle of redox cycling and electrode constructions. a) Scheme for redox cycling strategy in a 3D-LCNF based IDE setup: single mode (i) vs. dual mode (ii). b) IDE made from LCNFs as a flow-through system with a respective redox cycling scheme. c) Stacked electrodes (i) and the vertical scheme for redox cycling (ii). d) Exemplary cyclic voltammograms in dual mode and single mode measured with 1 mM $K_4[Fe(CN)_6]$ in 0.1 M K-PBS (pH 7) contained 0.1 M KCl for electrode constructions with (i) and without (ii) redox cycling.

for example, integrated into a syringe filter for both sample separation and detection.[28] Unlike in other works,[10,19,20] a nanofiber layer is applied as an insulating layer between the two bands of LCNF electrodes in which the thickness of the layer can be tuned via fiber collection time. The major challenge, in this case, was to create the thinnest possible nanofiber layer that still reliably prevented electrical shorting between the two band LCNF electrodes.

IDE fabrication and characterization

Investigating electrode designs

The writing process of the IDE electrodes relies on the carbonization of the PI nanofiber mat by a CO_2 laser which creates very focused energy on the substrate that subsequently triggers temperature-dependent processes. Such high temperatures can produce sintering and densification of the materials, which can further expand the size of the carbonized materials,[29] deviating from the original assigned dimension. The deviations may be negligible with electrode sizes in millimeter ranges, but it considerably affects the micrometer-sized electrodes, which commonly are designed as IDE with large working area within a limited space. Therefore, the effect of the laser fabrication process on the expansion of IDE fingers was thoroughly studied. In the design sketch, we drew the gaps wider than the fingers (see the labels on the x-axis in Figure 2a) to compensate for the expansion of the fingers due to laser-scribing and to avoid electrical short-circuit. If this is not done, the adjacent electrode fingers are prone to connect to each other, rendering unusable devices. The studies on the expansion shown in Figure 2a revealed that IDE fingers with narrower widths tend to expand more than wider ones (rel. to its original width, w_{f0}). The expansion of IDE fingers is in fact beneficial for redox cycling as greater ESA can be obtained, hence boosting detection sensitivity. Furthermore, the expansion consequently leads to the attainable narrower gap between the adjacent electrodes than the originally designed distance. Nevertheless, it is important to ensure that the expansion does not cause a connection between IDE fingers leading to short circuits, especially in the case of the narrowly designed initial gap width (w_{g0}). The results demonstrate the constraints of using CO_2 laser due to material expansion resulting in deviations of electrode design. The more precise processing and controlling may be achieved via a pulsed laser, which provides faster cooling (lower heat dissipation) than the normal CO_2 laser currently used in our group.[29]

We observed the resulting morphological structure of IDE fingers under an electron microscope, as shown in Figure 2b. Herein, we found a groove at the edge of each electrode finger. The groove could be attributed to the laser radiating the PI nanofibers at the beginning, where no LCNFs exist. The laser breaks down the nanofibers instead of properly carbonizing them. However, after the laser produced LCNFs in adjacent spots, the carbon nanomaterials may facilitate the absorption of CO_2 laser and further assist heat dissipation better than PI nanofibers alone. On the one hand, the grooves could be beneficial for the penetration of the solution in the depth of the fingers enabling more reactive sites. On the other hand, they could cause disruption in lateral flow. The size of the groove was found to be double the laser beam spot (25 µm) and could be maintained at around 50 µm for all the designed finger widths. Even though the IDE fingers with narrow widths, i.e., w_f of ca. 250 µm, will allow an accommodation of a greater number of IDE fingers, the space of the groove accounts for approx. 17% of each electrode finger, whereas they were only about 12.5% for the wider ones, i.e., w_f of ca. 400 µm. This

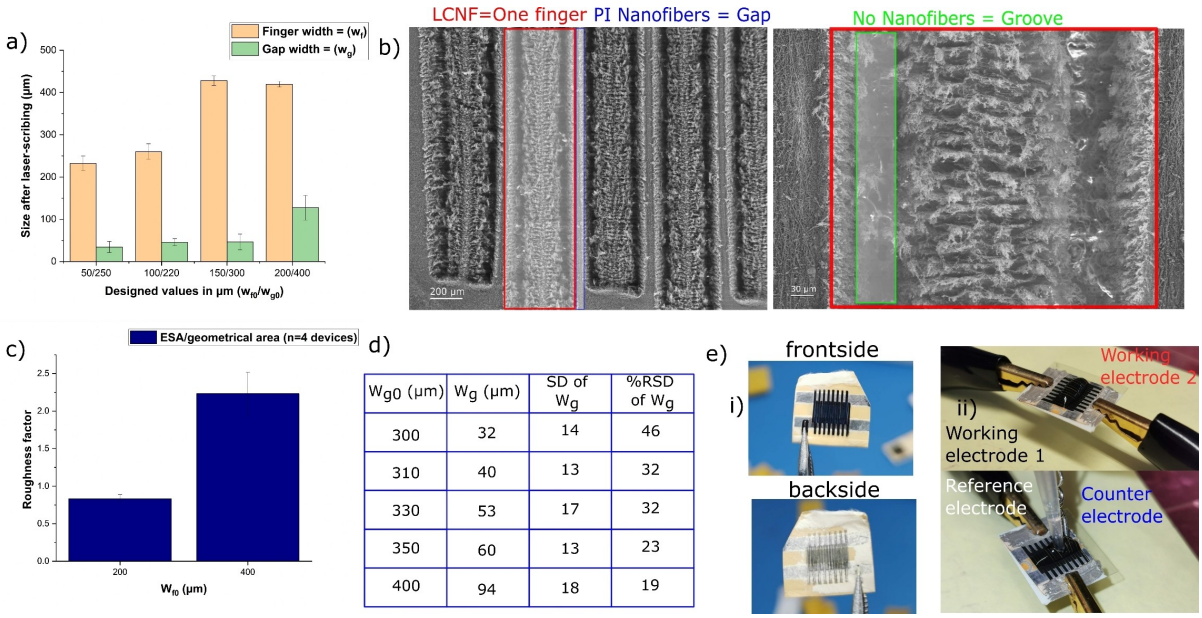

W_{g0} (µm)	W_g (µm)	SD of W_g	%RSD of W_g
300	32	14	46
310	40	13	32
330	53	17	32
350	60	13	23
400	94	18	19

Figure 2. Characterization of IDE array. a) Actual size of the fingers (w_f) and gap (w_g) versus the designed values ($n \geq 15$). b) SEM images of IDE fingers ($w_f \approx 400$ µm) showing the obtained microstructure in low (left) and high (right) magnification. c) Comparison of roughness factor between two different finger widths. d) Table illustrated the achievable gap distances from various designs where w_f was maintained at ca. 400 µm. e) Pictures of the IDE array device (i) and the setup for electrochemical characterization using external reference and counter electrodes (ii).

suggests that wider IDE fingers are more suitable as the effect of grooves on redox cycling could be minimized. Figure 2c also supported that the devices with wider electrode fingers significantly increase the roughness factor (the ratio of ESA to its geometrical area). For further studies, w_{f0} of 150 µm was therefore chosen where the w_f was ca. 400 µm and more reproducible in terms of manufacturing. With respect to the gap distances between IDE fingers shown in Figure 2d, the w_{g0} ranging from 310 to 400 µm were further investigated as the $w_{g0} = 300$ µm exhibited poor reproducibility. Figure 2e displays the photographs of IDE devices and the setup of electrochemical measurements.

Effect of electrode thickness and IDE substrate on redox cycling efficiency

As shown in Figure 2d, w_g of about 40 µm was the smallest gap accomplishable with our current fabrication approach and currently available instrumentation. In principle, apart from having a short distance between adjacent electrodes, large electrode widths, and a greater number of IDE fingers, elevating the height of electrodes and trapping analytes between adjacent fingers is considered an effective strategy in promoting redox cycling.[17,18,30] Electrode thickness in our work can be easily increased by extending fiber collection time (Figure 3a and Figure S2). As expected, the height of LCNF electrodes nicely correlated with the fiber collection time. In addition, Figure 3b illustrates a good correlation between the height of the electrode and the ESA. Here, 90 min-fiber collection time which provided an electrode height of ca. 100 µm, was the best candidate as the applied laser conditions allowed complete

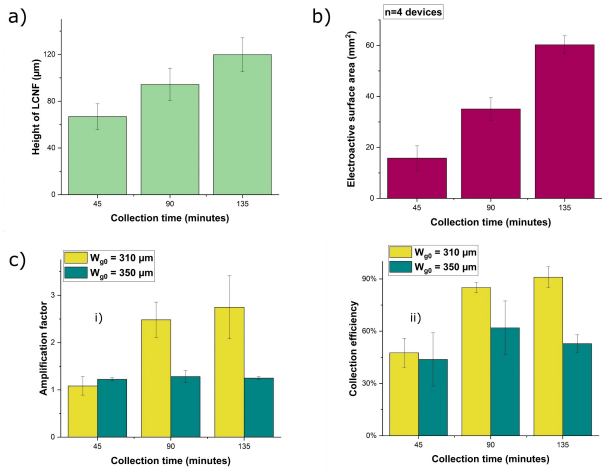

Figure 3. Influence of the fiber collection time. a) Height of the LCNFs determined from the side view of SEM images. b) The obtained ESA for LCNF electrodes with various thickness. c) Characterization of redox cycling efficiency where amplification factor (AF) (i) and collection efficiency (CE) (ii) were evaluated. For all investigations $n \geq 3$ different devices.

carbonization through the whole mat thickness, unlike the 135-min mat, and the fabrication is not too long.

When determining the redox cycling efficiency, it is found that the increase of electrode heights plays an important role in promoting signal amplification for electrodes with a w_g of about 40 µm ($w_{g0} = 310$ µm). As seen from Figure 3c, the electrodes from the 45-min mat did not result in redox cycling, i.e., AF of 1.0 and CE less than 50% were obtained. On the contrary, when elevating the electrode heights up to ca. 100 µm, redox cycling between adjacent electrodes took place, as can be seen from

the AFs greater than 1.0, and CE reached almost 100%. Nevertheless, increasing electrode thickness did not lead to better redox cycling efficiency for large inter-electrode distance, i.e., for the w_{g0} of 350 μm that resulted in a w_g of ca. 60 μm.

Parameters influencing redox cycling

One of the most important parameters influencing redox cycling is the distance between the adjacent fingers. Therefore, the achievable gap distances shown in Figure 2d were investigated towards their AF and CE (Figure 4a). As expected, the IDEs with smaller w_g can efficiently facilitate redox cycling in which w_g of ca. 50 μm (see also Figure 2d) was the maximum gap distance allowed. This behavior is predictable, as the larger gaps hinder the diffusion layers from overlapping. The shortest w_g of ca. 40 μm yielded the best AF and CE, which were about 3.5 and 95%, respectively. With the material cost (< 0.02 € per device), fabrication time (~10 minutes), inherent mass-production capability, and simplicity, the obtained redox cycling efficiency is considerably outstanding.

The thickness of the diffusion layer plays a crucial role in determining the redox cycling capability of the constructed devices. In principle, a successful redox cycling system requires an inter-electrode distance that is close to or smaller than the thickness of the diffusion layer. Therefore, parameters that govern the thickness of the diffusion layer were investigated. As can be seen from Figure 4b, low scan rates permitted the diffusion layer to grow for a longer time period, and thus, greater redox cycling efficiency was realized. Apart from the scan rate, the analyte concentration in bulk solution also affects the diffusion layer thickness (Figure 4c). Here, high analyte concentrations normally provide a steep concentration gradient, which results in a thinner thickness of the diffusion layer in comparison to lower concentrations when determined at the same distance from the electrode surface and at the same time. Therefore, it is not surprising that the redox cycling efficiency was better at low concentrations, i.e., the thinner diffusion layer from high analyte concentration hinders the overlapping of the diffusion layer between the two electrodes. Besides, this could be attributed to a high concentration of reactant already present at the electrode surface where the diffused recycling species exhibited minimal or negligible effect.

We further wanted to compare the LCNF electrodes to laser-scribed graphene (LSG) electrodes which have been originally fabricated from CO_2 laser exposure of PI or Kapton sheet.[31,32] In this study, we also investigated the effect of using a PI sheet on the resulting electrode dimensions after laser-scribing as well as their redox cycling efficiency, which has not yet been conducted. As shown in Figure S3a, with the same design of IDEs on nanofibers (Figure 2d), the gaps between two adjacent electrodes exceed 200 μm, which are unable to promote redox cycling. This emphasizes that the expansion of electrodes in the laser-exposed PI nanofibers (Figure 1a) considerably benefits the achievement of narrower gaps between adjacent electrodes. The greater expansion in the nanofiber mat could be possibly assisted by the following factors: 1) the random fibrous structure may lead to multiple scattering and reflecting events of the laser beam within nanofiber mat, and 2) the as-spun nanofibers are doped with iron, which can facilitate a greater dissipation of energy and thus yields more electrode expansion than that of the PI sheet. Furthermore, we attempted to achieve IDEs on PI film with w_g similar to that fabricated on the PI nanofibers. Herein, the w_{g0} of 130 and 150 μm were designed to obtain w_g in the range of ca. 50 μm (Figure S3b). The widths of IDE fingers fabricated on the film and nanofibers were adjusted to ca. 400 μm for a fair comparison. The IDE dimensions were given in Figure S3c–i and ii. Nevertheless, we were not able to get functional IDE devices from scribing on PI film using these dimensions, i.e., all devices were short-circuited. When measuring the resistances of IDEs on the opposite arrays fabricated from PI nanofibers, they were relatively high (10^5–10^6 ohms),

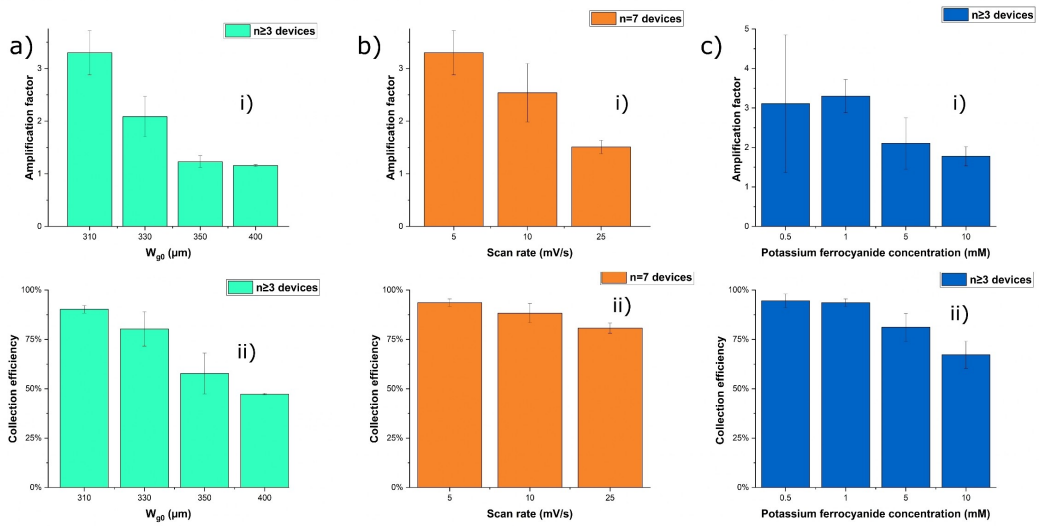

Figure 4. Optimization of parameters to maximize AF and CE of IDE array. a) Gap distance variation. b) Scan rate variation on an IDE with ca. 40 μm gap width. c) Concentration variation of ferrocyanide. Unless stated otherwise, a scan rate of 5 mV/s was applied.

whereas the planar LSG electrodes were in the range of a few hundred ohms as shown in Figure S3c–iii.

Chronoamperometry measurements

In addition to characterizing the redox cycling efficiency by CV, we performed a chronoamperometry study, which is widely used in electrochemical sensing. Figure 5a displays the current responses from the measurements in dual and single mode. Here, it is clear that using the generator and collector in the dual mode substantially enables a greater current response than that of the single mode. The relationship between w_{g0} and AF shown in Figure 5b is correlated well with the results obtained from the CV study (see also Figure 4a). With increasing the gap width, the AF decreases exponentially with an R^2 of 0.99. The well-known exponential behavior is observed, [33–36] which is caused by the shortening of the diffusion distance when decreasing the gap width. Furthermore, we evaluated the effect of w_{g0} on steady state current (i_{ss}) as well as the time to reach the steady state (t_{ss}) as shown in Figure 5c i–iii. As expected, the smaller inter-electrode distance resulted in greater i_{ss} and shorter t_{ss} than the larger ones.

Construction of stacked electrodes and characterizations

As earlier described, the efficiency of redox cycling depends on the distance in which redox species have to travel between the two electrodes. In the case of IDEs, the redox species horizontally travel between two adjacent electrodes. Therefore, the main limitation of IDE design is the lateral resolution of the applied fabrication methods. For high lateral resolution, such as in a few micrometers or nanometer range, the fabrication methods require technologies such as the electron beam, which is typically complicated and expensive.[6] An alternative strategy is to place electrodes on top of each other, where insulating space is created in between, avoiding the need for high-lateral resolution of fabrication. The spacer between the electrodes can be facilely tuned by adjusting the thickness of the insulating layer. We, therefore, constructed such electrode configuration for promoting redox cycling in LCNF electrode devices and compared their performance with the as-developed IDEs.

In this study, the stacked electrodes consist of two wide band LCNFs separated by a thin layer of a non-carbonized PI nanofiber mat, which acts as an insulating layer (Figure 1c–i). To fabricate the insulating layer from PI nanofibers, two strategies were initially investigated, i.e., 1) spinning nanofibers directly onto the as-prepared LCNF electrodes, or 2) spinning nanofiber separately on a blank filter paper and transferring the mat afterwards onto the LCNF electrodes. It was found that the former strategy is more practical and easier to fabricate than the latter one. We therefore proceeded further experiments with the first strategy, as shown in Figure 6. In order to study the effect of distance between electrodes on redox cycling efficiency, the fiber collection time was varied, as shown in Figure 6a. For this type of polymer, i.e., PI, and the current setup it is necessary to spin for at least 5 minutes to achieve a homogenous mat distributed on the as-fabricated LCNF electrodes. The steps of device assembly for stacked electrodes are given in Figure 6b. As shown in Figure S4, there is no significant

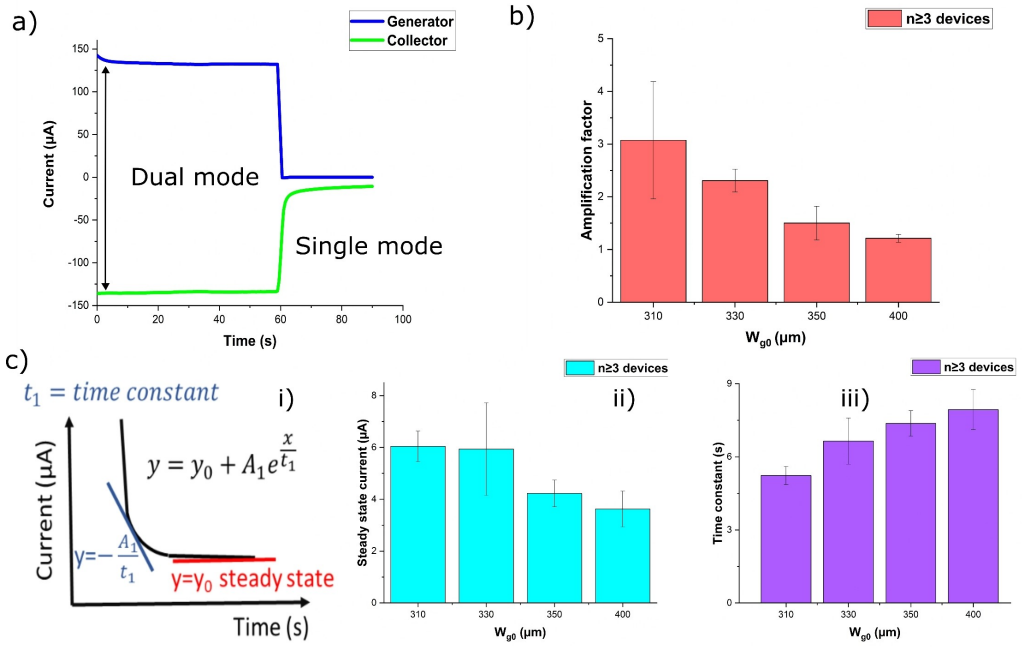

Figure 5. Effect of inter-electrode distance on electrochemical behavior in chronoamperometry. a) Exemplary chronoamperograms from generator and collector electrodes. b) Gap width variation and its corresponding AF. c) Evaluation of steady state current and time constant shown – model used for evaluation (i), steady state current (ii) and time to reach steady state (iii). Chronoamperogram of one device with ~400 µm fingers and ~40 µm gap distance measured with 1 mM ferrocyanide.

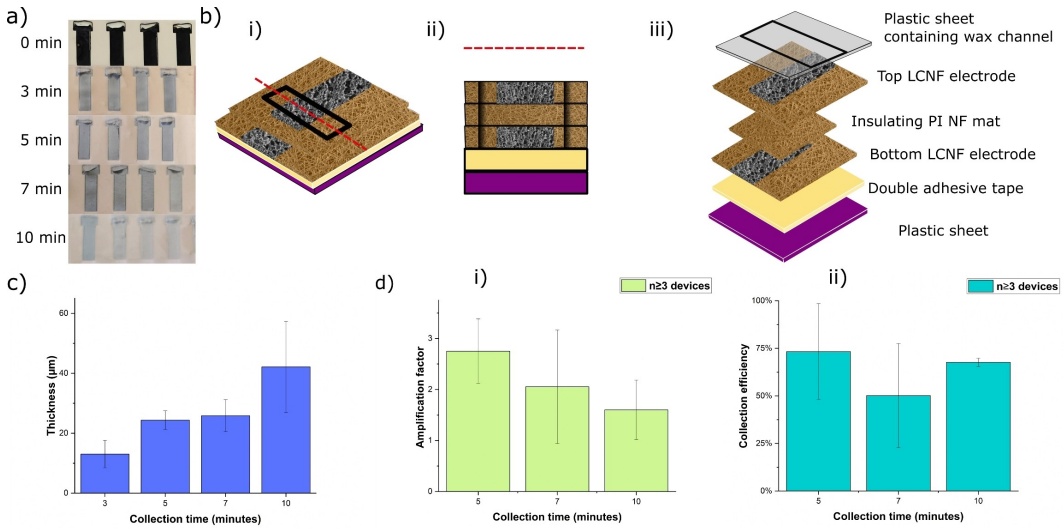

Figure 6. Fabrication of stacked electrodes. a) Photographs of the LCNF electrodes covered with nanofiber layer at various collection time. b) Schematic illustration of device assembly. c) Thickness of the nanofiber layer shown in a) determined from SEM images. d) Characterization of redox cycling efficiency of the nanofiber layers shown in a) and c) with respect to AF (i) and CE (ii).

distinction between the cyclic voltammograms of IDE and stacked electrodes.

The thicknesses of the nanofiber mat collected at various time points were determined from SEM images (Figure 6c and Figure S5). The dependency of redox cycling efficiency and fiber mat thickness was illustrated in Figure 6d. Interestingly, the AF for a stacked electrode with a separating fiber mat of ca. 40 μm thickness (10 min collection time) was only about half of the AF achieved with an IDE configuration with a similar inter-electrode distance (see also Figure 4a). In addition, the CE was approx. 25% less for the stacked electrodes. This result may indicate that IDE configuration possesses a higher number of available sites for redox cycling reaction (both vertical sides on each finger). In contrast, the reaction solely occurs at the surface of LCNFs facing the nanofiber mat in which the vertical thickness of electrodes did not significantly contribute to redox cycling. This further suggests that an electrospinning time of less than 90 min, e.g., 45 min, for LCNF fabrication, should be sufficient to enable redox cycling in stacked electrodes.

By collecting fibers for 3 to 7 min, an insulating layer of ~10–30 μm thickness could be achieved in the stacked electrode design. Nevertheless, although these layers were thinner than the smallest achievable gap width of 40 μm in the IDE design, they did not result in better redox cycling efficiency than in the best performing IDE device. This implies that the IDE array configuration is much more efficient in facilitating the recycling of redox species. Unlike the wide band stacked electrodes, the top electrode layer may not be in close contact with the entire area of the insulating layer after device assembly, thus hindering effective redox cycling reaction.

Finally, we observed that at scan rates of 5 and 10 mV/s, similar AFs were unexpectedly obtained for all of the stacked electrodes, which contained insulating layers with thicknesses of ~10–50 μm (data not shown). Unlike the IDE configuration shown in Figure 4b, the independence of scan rate in the stacked electrodes might be caused by the low nanofiber density of the insulating layer. The larger pores available in sparse fiber mats (3–10 min fiber collection time) may permit the traveling of redox species between electrodes easier than the smaller pores in dense fiber mats (90 min fiber collection time for IDE device).

The LCNFs have been demonstrated to produce redox cycling in both studied cases with comparable redox cycling efficiency (Table 1). Nevertheless, the IDE configuration is superior in terms of signal reproducibility and easier to fabricate. The poorer reproducibility of the signal exhibited in

Table 1. Comparison of the device construction approaches for redox cycling.

Factor	IDEs	Stacked electrodes
Max. amplification efficiency (fold)	~3.5	~3.5
Max. collection efficiency [%]	95	60
Min. gap distance [μm]	40	15
Reproducibility of signal (averaged RSD)[a]	Good (AF: 10% CE: 8%)	Fair (AF: 38% CE: 31%)
Reproducibility of device fabrication[b]	83% ($N=60$)	98% ($N=69$)
Total time spent for fabrication of each device [min]	~10	~15
Mass-production feasibility	high	moderate
Suitable application	lateral flow assay	vertical flow through system
Further improvement of AF and CE	likely (e.g., pulse laser)	unlikely

[a] The relative standard deviation (RSD) refers to Figure 4a and Figure 6d. [b] The number is obtained from functional devices (without short-circuit) in the same fabrication batch.

the stacked electrodes might be caused by the heterogeneity of the as-scribed LCNF electrodes, which leads to non-uniform distribution of the electric field during electrospinning of the insulating layer. Consequently, the electrodes possess nanofiber layers of different thickness even on the same mat substrate. Thus, the stacked electrodes displayed higher fluctuation in signals when compared to IDEs. Apart from the reproducibility of current signal represented by AF and CE, we determined the reproducibility of device fabrication. The IDE design yielded a larger proportion of unusable, i.e., short-circuited, devices compared to the stack design, possibly because this fabrication approach is more sensitive to the heterogeneity of nanofiber substrates. This heterogeneity is exemplary shown in Figure 2b (left), where the electrode finger on the very left side is wider than the others and also distorted. As a result, the distance between the adjacent electrodes becomes smaller when compared to the others. Possibly, the fiber mat in that area was less dense than the surroundings, causing the laser to leave a different carbonization footprint. The results suggest that the variation in the thickness or density of the fiber mat substrate before laser scribing is a key factor in governing the obtained reproducibility of device fabrication. Nevertheless, the present level of reproducibility leaves room for improvement. These issues can probably be overcome through more precise atmospheric control of the nanofiber spinning process, which may be available to our lab in the future. Although the instrumental control over relative humidity and temperature in our lab is currently subprime, the recent implementation of a rotating drum collector has significantly improved fiber mat homogeneity.

Although the redox cycling efficiency in this work is not as competitive as obtained from devices reported in the literature yet,[17,19,30] where 10–1000 times greater amplification was reported, we strongly believe that through adjusting the laser system with greater lateral resolution, an improvement of redox cycling efficiency is feasible while the instrumentation cost and fabrication steps involved can be kept at minimum with our strategy. However, the current findings clearly reveal the potential and constraints of the CO_2 laser in generating graphene porous electrodes for redox cycling.

The significant advantage of both constructions is its unique feature that can be exploited as a high-performing electrochemical transducer in any flow-through analytical device. For example, the IDEs can be implemented into microfluidic chips or lateral flow assays,[37] while the stacked electrodes are practical for vertical flow applications.[28,38] Similar to the well-known paper-based analytical devices (PADs), the as-developed IDE piece can be employed as a whole microfluidic system when combined with a wax channel to control the flow of solution, as previously demonstrated by our group.[1] Here, a channel filled with LCNFs and PI nanofibers can drive the solution flow by capillary force. In addition, the proposed redox cycling by IDE configuration is highly practical to be integrated with a nitrocellulose membrane on LFAs. Here, one side of the IDEs can be placed overlapping with one end of the membrane strip, where another end can be connected to an adsorbent pad for wicking the solution. The IDE-LFA coupled with chronoamperometric measurement, enabling simple, inexpensive, and sensitive point-of-care testing devices, can be envisioned, which is currently under investigation in our group as well. Furthermore, the vertical design is also highly practical for foldable paper-based analytical devices where the flow-through is likely to offer efficient washing through a capillary flow forced by a bottom adsorbent pad, which is suitable for label-based immunoassay electrochemical biosensors.[13] With both configurations, detection can be done either under stagnant or flow conditions. However, when detection is performed under flow conditions, the influences of the flow on redox cycling ability have to be carefully evaluated to ensure desired detection sensitivity.

It should also be noted that even though in this work we employed an external Ag/AgCl and Pt wire as a reference (RE) and auxiliary (AE) electrode, respectively, implementing LCNFs as RE and AE is also feasible. Our previous study has proven that AE and RE electrodes made from LCNF electrodes provide good stability and reliability.[1] Overall, the advantages of the systems lie not only in the achievable amplified performance but also in the simple and inexpensive fabrication, paving the way for the developing of affordable POC devices.

Conclusions

Nanofibers have been demonstrated as particular nanomaterials for POC and wearable devices since their porosity and flexibility can be used for mixing, wicking, and as breathable membranes. In this paper, electrodes made of carbonized nanofibers have been demonstrated as interdigitated or stacked electrodes to efficiently implement redox amplification for a highly sensitive strategy toward detecting electrochemically active molecules. Moreover, the as-described electrodes are not only fast, easy, and inexpensive to fabricate but also highly versatile, as their size, shape, and height are easily adjustable. Furthermore, the strategy to electrospin nanofibers onto electrodes can be exploited in terms of filtering, mixing, or capturing specific molecules which can be later detected at the electrode. The electrospun nanofibers on the electrodes could be adapted by choice of polymer to create gradients for wettability or design for repelling unwanted molecules. The as-described method is a significant development since most electrodes implemented in redox cycling schemes are expensive and complicated to fabricate. The substrate-free electrodes can be implemented in more complex detection strategies as lateral or vertical flow assays in combination with other nanofibers or porous membranes.

Experimental Section

Fabrication of PI nanofiber substrate

Nanofiber mats were prepared by electrospinning of a solution containing 15 wt% Matrimid 5218 (Huntsman Advanced Materials BVBA, Belgium) and 5 wt% (rel. to mass of Matrimid) iron (III) acetylacetonate (≥99.9% trace metals basis, Sigma-Aldrich, Ger-

many) dissolved in *N, N*-dimethylacetamide (Merck, Germany). The polymer solution was ultrasonicated for 30 minutes and afterward stirred overnight. The mats were collected for 90 minutes, unless stated otherwise, at a flow rate of 10 μl/min with a 15 cm tip-to-collector distance on filter paper (MN 616, Carl Roth, Germany). Depending on the environmental conditions the voltage was adjusted from 13–17 kV.

After electrospinning, conductive electrodes with desired patterns of carbon nanofibers were generated by a CO_2 laser (10.6 μm, VLS2.30, Universal Laser Systems Inc., USA). The as-generated electrodes were treated with oxygen plasma at 100 W for 3 minutes, to increase their hydrophilicity prior use. Our previous study has shown that such treatment conditions dramatically reduce the contact angles from 135 ± 2 to 35 ± 2, and 121 ± 6 to 16 ± 2 for LCNFs and PI nanofiber mats, respectively.[1] To confine the area of the electrodes, a hydrophobic channel was created via wax printing on a plastic sheet and melted on the as-scribed fiber mat by placing both facing each other on a hotplate. After melting the wax barrier, the LCNFs together with non-scribed fiber mat which adhered to the wax on plastic sheet was peeled off the filter paper and placed on double-sided adhesive tape to close the device. More details on device fabrication and assembling steps can be found in previous work.[1] The electrical contact pads to the LCNF electrodes were created by spreading silver paint on both sides.

PI nanofiber mat substrates for LCNF fabrication were prepared according to the previous protocol without modifications for both designs.[1] However, in laser pyrolysis process of IDE array high power density focusing optics (HPDFO) lens was employed instead of 2-inch lens because it provides a smaller focal spot size (25 μm and 127 μm for HPDFO and 2-inch lens, respectively). Hence, widths of IDE finger in the range of a few tens of micrometers can be generated, enabling the generation of several electrode fingers within an array and confined space. The power and speed of CO_2 laser were adjusted for HPDFO lens to obtain functional IDE-LCNFs. However, with the stacked electrode design, typical 2-inch lens was sufficient as high lateral resolution is not concerned.

Electrochemical characterization

The electrochemical measurements were performed using a μStat 400 BiPotentiotat (DropSens S.L., Spain). Potassium ferrocyanide ($K_4[Fe(CN)_6]$) with 0.1 M potassium chloride (KCl) in 0.1 M K-phosphate buffered saline (pH 7) was used as a model redox species owing to its excellent electrochemical reversibility on the LCNF electrodes. Ag/AgCl and a Pt wire were used as a reference and counter electrode, respectively. The fabricated devices were placed on a moveable lab stage, and the silver painted contact areas were connected to crocodile clamps for WE1 and WE2 (see Figure 2e). A drop of 50 μL electrolyte was pipetted onto the sensing area after which the reference electrode (Ag/AgCl topped with agar-plug pipette tip) and counter electrode (Pt wire, coiled around RE) were immersed into the drop. To determine redox cycling efficiency, cyclic voltammograms in stagnant solution were recorded in dual mode, one working electrode serves as a generator and a second one as a collector.[17] The generator is swept from −0.2 to 0.6 V, while the collector is held constant at −0.25 V. For the chronoamperometric measurements one of the working electrodes was held at the oxidation potential and the other one at the reduction potential. The oxidation potential was fixed at 0.4 V (see also the CV shown in Figure S1) and the reduction at −0.25 V.

To determine electroactive surface area (ESA), a set of electrode fingers was used. Cyclic voltammetry was performed at 25, 50, 75, 100, 150 and 250 mV/s. The anodic peak intensity at each scan rate was plotted against square root of scan rate, yielding a slope for the estimation of ESA following Randles-Sevcik equation (at 25 °C) shown below.

$$I_{p,a} = (2.69\times10^5)n^{\frac{3}{2}}ACD^{\frac{1}{2}}\nu^{\frac{1}{2}} \quad (1)$$

where $I_{p,a}$ is the peak current [A], A is the ESA of the electrode investigated [cm^2], D is the diffusion coefficient of $K_4[Fe(CN)_6]$ (7×10^{-6} cm^2/s),[39] n is the number of electrons transferred in the redox reaction, C is the concentration of the analyte in the bulk solution [mol/cm^3], and ν is the scan rate [V/s].

The amplification factor and collection efficiency were determined as following.

$$\text{Amplification factor} = \frac{I \text{ at 600 mV of gen. in } \textbf{dual mode}}{I \text{ at 600 mV of gen. in } \textbf{single mode}} \quad (2)$$

$$\text{Collection efficiency } [\%] = \frac{I \text{ at 600 mV of } \textbf{col}. \text{ in dual mode}}{I \text{ at 600 mV of } \textbf{gen}. \text{ in dual mode}} \times 100 \quad (3)$$

Morphology characterization

The nanofibers were imaged using scanning electron microscopy (Zeiss/LEO 1530, Germany) at 5 kV. After the cutting of the samples, they were sputtered with gold for 30 s (≈7 nm layer thickness) and placed on specimen stubs. A light microscope from KERN Optics Germany was used to determine the gap width and finger width.

Acknowledgements

This work was funded by the Deutsche Forschungsgemeinschaft (DFG, German Research Foundation) Projektnummer 457100614. We also would like to thank Projekt DEAL for Open Access funding.

Conflict of Interests

The authors declare no conflict of interest.

Data Availability Statement

The data that support the findings of this study are available from the corresponding author upon reasonable request.

Keywords: redox cycling · point-of-care devices · electrochemical sensor · laser-induced carbon nanofibers · flow-through device

[1] A. Perju, A. J. Baeumner, N. Wongkaew, *Microchim. Acta* **2022**, *189*, 424.
[2] M. A. Ali, K. Mondal, Y. Jiao, S. Oren, Z. Xu, A. Sharma, L. Dong, *ACS Appl. Mater. Interfaces* **2016**, *8*, 20570–20582.
[3] N. Baig, T. A. Saleh, *Microchim. Acta* **2018**, *185*, 283.
[4] X. J. Huang, A. M. O'Mahony, R. G. Compton, *Small* **2009**, *5*, 776–788.

[5] P. M. Lewis, L. B. Sheridan, R. E. Gawley, I. Fritsch, *Anal. Chem.* **2010**, *82*, 1659–1668.
[6] B. Wolfrum, E. Kätelhön, A. Yakushenko, K. J. Krause, N. Adly, M. Hüske, P. Rinklin, *Acc. Chem. Res.* **2016**, *49*, 2031–2040.
[7] T. Šafarik, A. Karajić, S. Reculusa, P. N. Bartlett, N. Mano, A. Kuhn, *Adv. Funct. Mater.* **2023**, *33*, 2210638.
[8] E. O. Barnes, G. E. M. Lewis, S. E. C. Dale, F. Marken, R. G. Compton, *Analyst* **2012**, *137*, 1068–1081.
[9] M. Hu, I. Fritsch, *Anal. Chem.* **2016**, *88*, 5574–5578.
[10] S. Yamamoto, S. Uno, *Sensors* **2018**, *18*, 730.
[11] E. Kätelhön, B. Wolfrum, *Rev. Anal. Chem.* **2012**, *31*, 7–14.
[12] N. Wongkaew, P. He, V. Kurth, W. Surareungchai, A. J. Baeumner, *Anal. Bioanal. Chem.* **2013**, *405*, 5965–5974.
[13] G. Y. Lee, J. H. Park, Y. W. Chang, S. Cho, M. J. Kang, J. C. Pyun, *ACS Sens.* **2018**, *3*, 106–112.
[14] V. Matylitskaya, S. Kasemann, G. Urban, C. Dincer, S. Partel, *J. Electrochem. Soc.* **2018**, *165*, B127-B134.
[15] J. S. Shim, M. J. Rust, C. H. Ahn, *J. Micromech. Microeng.* **2013**, *23*, 035002.
[16] J. Il Heo, Y. Lim, H. Shin, *Analyst* **2013**, *138*, 6404.
[17] R. R. Kamath, M. J. Madou, *Anal. Chem.* **2014**, *86*, 2963–2971.
[18] N. Honda, M. Inaba, T. Katagiri, S. Shoji, H. Sato, T. Homma, T. Osaka, M. Saito, J. Mizuno, Y. Wada, *Biosens. Bioelectron.* **2005**, *20*, 2306–2309.
[19] N. Y. Adly, B. Bachmann, K. J. Krause, A. Offenhäusser, B. Wolfrum, A. Yakushenko, *RSC Adv.* **2017**, *7*, 5473–5479.
[20] S. Park, J. H. Park, S. Hwang, J. Kwak, *Electrochem. Commun.* **2016**, *68*, 76–80.
[21] K. Muzyka, G. Xu, *Electroanalysis* **2022**, *34*, 574–589.
[22] G. Li, *J. Appl. Phys.* **2020**, *127*, 010901.
[23] T. Han, A. Nag, R. B. V. B. Simorangkir, N. Afsarimanesh, H. Liu, S. C. Mukhopadhyay, Y. Xu, M. Zhadobov, R. Sauleau, *Sensors* **2019**, *19*, 13–22.
[24] Y. Okamoto, Y. Takei, T. V. Nguyen, S. Kano, T. Kobayashi, M. Ichiki, *IEEE Symp. Mass Storage Syst. Technol.* **2022**, *January*, 527–530.
[25] A. Ray, J. Roth, B. Saruhan, *Molecules* **2022**, *27*, 329.
[26] A. Velasco, Y. K. Ryu, A. Hamada, A. De Andrés, F. Calle, J. Martinez, *Nanomaterials* **2023**, *13*, 788.
[27] M. Simsek, K. Hoecherl, M. Schlosser, A. J. Baeumner, N. Wongkaew, *ACS Appl. Mater. Interfaces* **2020**, *12*, 39533–39540.
[28] P. Chorti, A. P. Kazi, A.-M. J. Haque, M. Wiederoder, D. C. Christodouleas, *Sens. Actuators B* **2022**, *351*, 130965.
[29] D. Zhang, B. Gökce, S. Barcikowski, *Chem. Rev.* **2017**, *117*, 3990–4103.
[30] J. Il Heo, Y. Lim, H. Shin, *Analyst* **2013**, *138*, 6404–6411.
[31] A. Behrent, C. Griesche, P. Sippel, A. J. Baeumner, *Microchim. Acta* **2021**, *188*, 59.
[32] J. Lin, Z. Peng, Y. Liu, F. Ruiz-Zepeda, R. Ye, E. L. G. Samuel, M. J. Yacaman, B. I. Yakobson, J. M. Tour, *Nat. Commun.* **2014**, *5*, 5714.
[33] A. J. Bard, T. V. Shea, J. A. Crayston, G. P. Kittlesen, M. S. Wrighton, *Anal. Chem.* **1986**, *58*, 2321–2331.
[34] K. Aoki, M. Morita, O. Niwa, H. Tabei, *J. Electroanal. Chem.* **1988**, *256*, 269–282.
[35] S. Partel, C. Dincer, S. Kasemann, J. Kieninger, J. Edlinger, G. Urban, *ACS Nano* **2016**, *10*, 1086–1092.
[36] O. Niwa, M. Morita, H. Tabei, *Anal. Chem.* **1990**, *62*, 447–452.
[37] A. Perju, N. Wongkaew, *Anal. Bioanal. Chem.* **2021**, *413*, 5535–5549.
[38] P. Chen, M. Gates-Hollingsworth, S. Pandit, A. Park, D. Montgomery, D. AuCoin, J. Gu, F. Zenhausern, *Talanta* **2019**, *191*, 81–88.
[39] A. G. M. Ferrari, C. W. Foster, P. J. Kelly, D. A. C. Brownson, C. E. Banks, *Biosensors* **2018**, *8*, 53.

Manuscript received: June 12, 2023
Revised manuscript received: July 14, 2023
Version of record online: ■■, ■■

RESEARCH ARTICLE

Laser-induced carbon nanofibers are used to create porous freestanding electrode systems for redox cycling. Either by closely spacing the interdigitated electrodes carbonized directly onto the nanofibrous network, or by fabricating an additional nanofibers layer onto the electrodes, amplification via redox cycling was achieved in these new approaches, facilitating a flow-through electroanalytical device with favorable sensitivity.

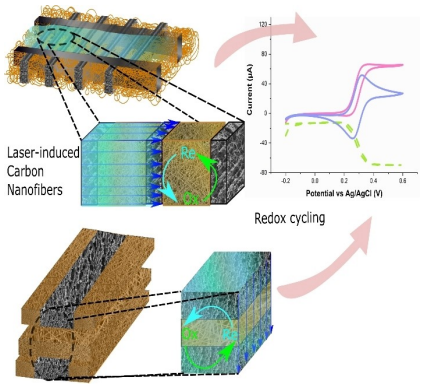

*Dr. A. Perju, Dr. N. Wongkaew**